Helmholtz-Zentrum Dresden-Rossendorf (HZDR)

Study of the Interaction of Eu3+ with Microbiologically Induced Calcium Carbonate Precipitates using TRLFS

Johnstone, E. V.; Hofmann, S.; Cherkouk, A.; Schmidt, M.;

Study of the Interaction of Eu^{3+} with Microbiologically Induced Calcium Carbonate Precipitates using TRLFS

Journal:	*Environmental Science & Technology*
Manuscript ID	es-2016-034346.R1
Manuscript Type:	Article
Date Submitted by the Author:	04-Oct-2016
Complete List of Authors:	Johnstone, Erik; Helmholtz-Zentrum Dresden-Rossendorf, Institute of Resource Ecology Hofmann, Sascha; Helmholtz-Zentrum Dresden-Rossendorf Cherkouk, Andrea; Helmholtz-Zentrum Dresden-Rossendorf, Institute of Resource Ecology Schmidt, Moritz; Helmholtzzentrum Dresden-Rossendorf, Institute of Resource Ecology

SCHOLARONE™
Manuscripts

Study of the Interaction of Eu^{3+} with

Microbiologically Induced Calcium Carbonate

Precipitates using TRLFS

Erik V. Johnstone, Sascha Hofmann, Andrea Cherkouk, and Moritz Schmidt*

Helmholtz-Zentrum Dresden - Rossendorf, Institute of Resource Ecology, Bautzner Landstrasse
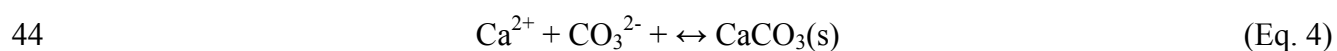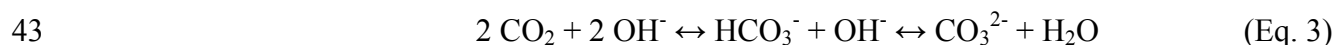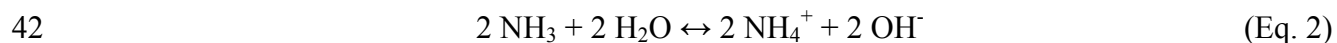400, 01328 Dresden, Germany.

ABSTRACT

The microbial induced biomineralization of calcium carbonate using the ureolytic bacterium
Sporosarcina pasteurii in the presence of trivalent europium, a substitute for trivalent actinides,
was investigated by time resolved laser-induced fluorescence spectroscopy (TRLFS) and a
variety of physicochemical techniques. Results showed that the bacterial-driven hydrolysis of
urea provides favorable conditions for $CaCO_3$ precipitation and Eu^{3+} uptake due to subsequent
increases in NH_4^+ and pH in the local environment. Precipitate morphologies were characteristic
of biogenically formed $CaCO_3$ and consistent with the respective mineral phase compositions.
The formation of vaterite with some calcite was observed after one day, calcite with some
vaterite after one week, and pure calcite after two weeks. The presence of organic material
associated with the mineral was also identified and quantified. TRLFS was used to track the

18   interaction and speciation of Eu^{3+} as a molecular probe with the mineral as a function of time.

19   Initially, Eu^{3+} is incorporated into the vaterite phase, while during $CaCO_3$ phase transformation

20   Eu^{3+} speciation changes resulting in several species incorporated in the calcite phase either

21   substituting at the Ca^{2+} site or in a previously unidentified, low-symmetry site. Comparison of

22   the biogenic precipitates to an abiotic sample shows mineral origin can affect Eu^{3+} speciation

23   within the mineral.

24   **INTRODUCTION**

25   Biomineralization is the process by which living organisms produce minerals. This phenomenon

26   occurs universally throughout the biological kingdom, yielding a variety of minerals with

27   different compositions, morphologies, and properties. There are three categories of

28   biomineralization: biologically-controlled, biologically-influenced, and biologically induced

29   mineralization.[1-3] For the latter, an array of microorganisms has been reported to induce the

30   precipitation of calcium carbonate minerals, i.e., carbonatogenesis, also referred to as microbial

31   induced calcium carbonate precipitation (MICP).[4] Over 40 different microorganisms have been

32   reported to induce $CaCO_3$ precipitation.[5] Organisms associated with the nitrogen cycle that are

33   able to induce biomineralization, e.g., ammonification of amino acids, nitrate reduction, or urea

34   hydrolysis, have been the most studied.[6-8] Hydrolyzing urea using ureolytic bacteria has proven

35   to be a simple and efficient method for precipitating $CaCO_3$. Mechanistically, when urea

36   (H_2NCONH_2) is metabolized it is converted to NH_3 and dissolved inorganic carbon (Eq. 1),

37   which equilibrate in water increasing the alkalinity (Eq. 2 and 3). The increased pH of the

38   solution, is buffered by the formation of NH_4^+ ($pK_a = 9.24$), but ultimately leads to precipitation

39   of $CaCO_3$ in the presence of Ca^{2+} (Eq. 4).[6,9-12] Previous studies have shown that varying

40   polymorphs of $CaCO_3$, typically vaterite and calcite, can be produced using this technique.[13]

41    $$H_2NCONH_2 \rightarrow 2\ NH_3 + CO_2 \qquad \text{(Eq. 1)}$$

42    $$2\ NH_3 + 2\ H_2O \leftrightarrow 2\ NH_4^+ + 2\ OH^- \qquad \text{(Eq. 2)}$$

43    $$2\ CO_2 + 2\ OH^- \leftrightarrow HCO_3^- + OH^- \leftrightarrow CO_3^{2-} + H_2O \qquad \text{(Eq. 3)}$$

44    $$Ca^{2+} + CO_3^{2-} + \leftrightarrow CaCO_3(s) \qquad \text{(Eq. 4)}$$
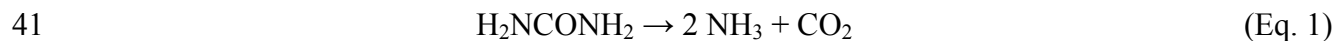
45   MICP has gained much interest as a geobiological tool for addressing a variety of environmental,

46   agricultural, and architectural problems.[4,14-16] For example, these include soil and water

47   remediation, formation of underground barriers, lake and reservoir sealing, concrete and

48   limestone restoration, and CO_2 sequestration.[4,15] From an environmental remediation focus, the

49   use of MICP has been suggested for the sequestration, retardation, or even complete removal of

50   toxic and harmful contaminants. These contaminants include toxic metals[17,18] and radioactive

51   elements, e.g., U and ^{90}Sr.[13] Particularly concerning these radioelements, most studies have been

52   aimed at the cleanup and removal of ^{90}Sr from contaminated nuclear legacy sites, which include

53   the proposed use of bioengineering techniques such as pulse-flow injection.[19-21] Results have

54   shown effective Sr^{2+} uptake and immobilization into biogenic $CaCO_3$. Using XAS Fujita et al.

55   observed the formation of a solid solution with Sr^{2+} substitution at the Ca^{2+} site within calcite

56   lattice.[20]

57   The long-lived, highly radiotoxic transuranic elements, i.e., neptunium, plutonium, americium,

58   and curium, as well as some lanthanide fission products, e.g. ^{155}Eu,[22] are a major environmental

59   concern. They are man-made elements or nuclides, resulting from nuclear processes that have

60   been or will be introduced into the biosphere during geologic disposal, nuclear accidents, and in

61   nuclear weapons fallout.[23,24,25] The progressively widespread use of lanthanides in technological

62   devices and as medical imaging agents also increases possibilities of contamination of the

63   environment.[26] Additionally, some trivalent lanthanides/actinides exhibit similar size and

64   coordination geometry to Ca^{2+}, which allows these elements to follow Ca^{2+} in biological systems,

65   e.g. by incorporation into bones [Holliday et al.].[27] When considering their radio- and

66   chemotoxicities, this behavior can be particularly harmful for biota, thus schemes for their reuse

67   and/or disposal should be developed.

68   Previous studies have determined that trivalent americium[28] and curium[29] as well as their

69   homologous lanthanides[30-32] are strongly partitioned into phases of $CaCO_3$. The interactions of

70   these elements with $CaCO_3$ are often dominated by surface sorption or incorporation, where

71   incorporation can occur either in the bulk structure or at the Ca^{2+} position in the crystal lattice via

72   substitution.[32-34] Although an appreciable amount of natural calcite is of biogenic origin and can

73   host a substantial amount of Eu^{3+},[35] never have the interactions of trivalent rare earth or actinide

74   elements with biogenic $CaCO_3$ been systematically studied. Comparatively, the bio(apatite)

75   system has been investigated, and it was revealed that these elements interact with biogenic

76   apatite considerably different than with the inorganically derived mineral. Results showed that

77   Eu^{3+} was found incorporated in the grain boundaries of the lattice and not at either of the Ca^{2+}

78   sites within the mineral as was previously reported. This difference in structural localization can

79   have significant implications when considering actinide sequestration in human bone.[36,37] With

80    $CaCO_3$ ubiquitously occurring throughout the bio- and geosphere, found in shells and skeletal

81   components and in the mineralogy of many nuclear repositories, this raises the question if similar

82　　effects may be found for biogenic $CaCO_3$, i.e., if there are differences in how trivalent actinides

83　　and lanthanides interact with abiotic and biotic $CaCO_3$.

84　　Time resolved laser-induced fluorescence (TRLFS) is an important and versatile tool for

85　　studying mineral interactions with luminescent trivalent actinides and lanthanides, i.e., Eu, Am,

86　　and Cm.[23,28,29,38,39] This characterization tool allows the site-selective excitation of a fluorescent

87　　probe in low concentrations ($\sim 10^{-7}$ M Eu^{3+}) to determine discrete species present with a mineral.

88　　From this, detailed information of probe symmetry from characteristic emission band splittings

89　　and extent of hydration from measured fluorescent decay lifetimes can be determined for the

90　　differentiation of species that are either surface sorbed or incorporated in the mineral.[40] In turn,

91　　this may help to evaluate the stability of the formed solid solution more accurately as well as the

92　　geochemical properties of trivalent actinides and lanthanides associated with $CaCO_3$.

93　　The aim of this study was to gain a better understanding of the process of biomineralization of

94　　$CaCO_3$ and how trivalent actinide or lanthanide elements could potentially interact with it.

95　　Calcium carbonate was precipitated via ureolysis using *Sporosarcina pasteurii*, an archetypal

96　　ureolytic bacterium, in the presence of Eu^{3+} and studied using a variety of analytical techniques.

97　　TRLFS was used to investigate the behavior of Eu^{3+} with the resulting mineral. The effect of

98　　biogenic components incorporated into the mineral on Eu^{3+} speciation was compared to an

99　　abiotic sample synthesized under similar conditions.

100　　**EXPERIMENTAL**

101　　**Culturing and Inoculation.** The strain *Sporosarcina pasteurii* (DSM33, ATC11859) was

102　　cultured in CASO medium (Merck 105458) (15 g/L peptone from casein, 5 g/L peptone from

103　　soymeal, 5 g/L NaCl, pH = 7.3) amended with 20 g/L urea at 30 °C on a rotary shaker (80 rpm)

104   overnight. For the inoculation, cultures were transferred into fresh media and grown at 30 °C for

105   approximately 15 hours. The bacteria were harvested from a 50 mL aliquot using a rotary

106   centrifuge (8,820 rcf) for 15 minutes. The supernatant was removed and the resulting cell pellet

107   was resuspended and washed two times with 50 mL of medium containing 20 g/L urea, 10 g/L

108   NH_4Cl, and 2.12 g/L Na_2CO_3 in MilliQ filtered water and pH adjusted to 5.6. The cell pellet was

109   then diluted in the same medium until an optical density reading at 600 nm (OD_{600}) using a

110   spectrophotometer (Cary 50 Bio) with a 1 cm path length of 0.40 ± 0.02.

111   **Mineralizing Medium.** The $CaCO_3$ mineralizing medium used was similar to that reported by

112   Stocks-Fischer (1999).[6] This was prepared by mixing of two solutions: a first solution of 3.0 g

113   bacterial nutrient broth in 800 mL of MilliQ filtered water at pH adjusted to 5.6 with the

114   dropwise addition of concentrated HCl(aq), which was then autoclaved. A second solution was

115   prepared by dissolving 20 g urea, 10 g NH_4Cl, and 2.12 g Na_2CO_3 in 180 mL of MilliQ filtered

116   water and pH adjusted to 5.6. To this solution 3.7 g $CaCl_2 \cdot 2H_2O$ and a 100 μL aliquot of a

117   1.0×10^{-3}M solution of $EuCl_3 \cdot 6H_2O$ were added, the pH was readjusted again to 5.6, and the final

118   volume adjusted to 200 mL. The second solution was filter sterilized through a 0.2 μm filter and

119   combined with the first for a final stock solution containing 3.g/L nutrient broth, 20 g/L urea, 10

120   g/L NH_4Cl, and 2.12 g/L Na_2CO_3, 3.7 g/L $CaCl_2 \cdot 2H_2O$, and 1.0×10^{-7} M $EuCl_3 \cdot 6H_2O$.

121   **$CaCO_3$ Precipitation Experiments with Europium.** Experiments were performed using sterile

122   handling techniques under aerobic conditions. The mineralizing medium stock (150 mL) was

123   transferred into two different 250 mL Erlenmeyer flasks each, and 1 mL of the previously

124   described inoculum containing *S. pasteurii* was added to one of the flasks for a calculated

125   starting OD_{600} = 0.003 and a 1 mL aliquot of medium containing no bacteria added to the

126   control. The bacterial and abiotic control flasks were kept at 30 °C on a rotary shaker (80 rpm).

127   Samples (1 mL) were collected from both flasks at varying times throughout the duration of the

128   experiment into 1.5 mL centrifuge tubes, centrifuged at 16,100 rcf at 25 ºC for 5 minutes, and the

129   supernatants were removed. The pH was determined immediately, while samples for inductively

130   coupled plasma mass spectrometry (ICP-MS) measurements and determination of $[NH_4^+]$ were

131   stored at 4 ºC until measured. In addition, mineral formed in the flasks containing bacteria was

132   sampled with a pipette during the duration of the experiment at different times and monitored

133   with light microscopy. Experiments were run for durations of either one day, one week, or two

134   weeks. All experiments were performed in triplicate.

135   At the end of each experiment, the supernatant containing the biomass was removed from the

136   precipitate by decantation. Subsequently, the reaction flask containing was scraped with a

137   sterilized glass rod to remove any adhered precipitate and the precipitate was transferred into a

138   sterile centrifuge tube. The precipitate was washed twice with MilliQ water and twice with

139   acetone, lightly capped, and air-dried. Precipitate from the triplicate samples for one day, one

140   week, and two weeks were then characterized using a variety of physicochemical instrumental

141   methods unless stated otherwise.

142   Because it was of interest to distinguish between the impact of biogenic components and that of

143   the growth medium on the interaction of Eu^{3+} with the mineral, an abiotic precipitate was

144   synthesized for comparison with the biogenic $CaCO_3$. In the absence of bacteria, mineralization

145   was induced by dropwise titration of the Eu^{3+}-containing mineralizing medium (150 mL) with an

146   NaOH solution until pH ~ 9.2. The resulting sample was incubated for 10 days at 30 ºC on a

147   rotary shaker (80 rpm) and the precipitate was harvested using the same techniques as above.

148   The resulting sample, which will be referred to as the abiotic precipitate, was analyzed by

149   TRLFS

150   **Characterization Methods**. *Time Resolved Laser-Induced Fluorescence (TRLFS)*. TRLFS can

151   be used for determining the local coordination environment of the Eu^{3+} ion. The non-

152   degenerative (J = 0) excitation of the ground state $^7F_0$ to the excited state $^5D_0$ yields a single peak

153   for each respective species. Excitation spectra can be produced by probing the sample with

154   varying excitation wavelengths and measuring the integrated fluorescence yield. For the Eu^{3+}

155    $^7F_0 \rightarrow {}^5D_0$ transition an appropriate excitation wavelength window ranges from 577 nm to

156   582 nm. Direct excitation of each species yields a characteristic emission spectrum and

157   fluorescence lifetime. Splitting patterns of the $(^5D_0 \rightarrow {}^7F_1)$ and $(^5D_0 \rightarrow {}^7F_2)$ bands can be used to

158   determine the local site symmetry of the Eu^{3+} ion which can be compared to the crystallography

159   of the host mineral.[40] Higher splitting patterns of these transitions are indicative of lower site

160   symmetry with a maximum splitting equal to (2J + 1).[40]

161   Fluorescence lifetimes can be empirically correlated to the degree of hydration where shorter

162   lifetimes, i.e., < 1700 μsec, are a result of non-radiative energy transfer to OH-oscillator

163   vibrations, and longer lifetimes, i.e., ≥ 1700 μsec, indicate no bound water associated with the

164   Eu^{3+} ion. Employing Horrocks and Sudnick's equation (Eq. 5) the decay constant k (1/ τ)

165   correlates to the amount of quenching water molecules where τ is in milliseconds.[41]

166 $$n(H_2O) = 1.07k - 0.62 \qquad \text{(Eq. 5)}$$

167   The measured lifetime and degree of hydration provide insight into the speciation of Eu^{3+} either

168   in solution or in the presence of a solid interface. For example, the Eu^{3+} aquo-ion yields a low

169   fluorescence lifetime, i.e., τ = 110 μsec, that equates to 9 H_2O in its inner coordination sphere,

170   whereas when it is fully incorporated into the crystal lattice of a mineral, such as calcite, longer

171   lifetimes are obtained, i.e., τ > 3600 μsec, equivalent to 0 H_2O present.[32]

172   TRLFS was performed using a pulsed (10 Hz) Nd:YAG (Spectra Physics, 532 nm) pumped dye

173   laser (Radiant Dyes). The laser dye Pyrrhomethene 580 was used for direct excitation of Eu^{3+} in

174   the range from 575–582 nm. The laser wavelength and power were monitored using a wavemeter

175   (High Finesse WS-5) ($>10^{-5}$ nm accuracy) and power meter (Newport 1918-R), respectively.

176   Fluorescence measurements were detected by an optical multichannel analyzer that consists of a

177   monochromator with 300/600/1200 lines/mm gratings (Acton SpectraPro 300i) and an

178   intensified CCD (Princeton Instruments). Maximum resolution at 300 and 1200 lines/mm was

179   measured to be 0.9 and 0.2 nm, respectively. The detection system was calibrated with a neon

180   lamp (Pen Ray 6032). The samples were cooled to ~ 10 K by a helium refrigerated cryostat

181   (CTI-cryogenics) to improve resolution. To avoid camera exposure to the direct laser beam, the

182   minimum gate delay between laser pulse and camera gating was set to 1.0 μs. The gate width of

183   the camera was fixed at 10 ms to ensure the collection of the entire fluorescence signal.

184   Fluorescence lifetime measurements were made with a delay time step between 50 and 150 μs

185   and a total of 100 steps were taken for each lifetime measurement.

186   *Microscopy and Mineral Composition Analysis*. Precipitates for light microscopy imaging were

187   directly sampled from solution, separated from the supernatant, and washed with sterile MilliQ

188   water. The samples were resuspended in water (~4 μL) and pipetted onto glass slide, covered

189   with a glass coverslip, and imaged using an Olympus BX61 light microscope. Samples for

190   scanning electron microscopy (SEM)/energy dispersive X-ray spectroscopy (EDX) were

191   prepared by transferring the precipitate in MilliQ water onto a silicon wafer and dried in a

192   desiccator at ambient temperature. The samples were imaged with a Zeiss EVO 50 SEM

193   equipped with a Bruker AXS QUANTAX 200 EDX. Mineral phase composition was determined

194   with a Bruker D8 powder X-ray diffractometer or a RIGAKU MiniFlex 600. Precipitates were

195   pulverized in an agate mortar and the resulting powders were evenly dispersed on a low-

196   background silicon wafer and measured from 18º to 50º 2θ with a step size of 0.02º 2θ. Thermal

197   gravimetric analyses (TGA) were conducted on one representative of the triplicate samples from

198   the one day, one week, and two week experiments. Samples were measured in a Mettler Toledo

199   TGA with a TG 50 furnace unit. A sample of 20 to 40 mg were heated in a ceramic crucible

200   under a nitrogen atmosphere (100 ml/h) over the range of 35 to 850 ºC at a rate of 10 ºC/sec.

201   Multi-point N_2-BET surface area of the precipitate after two weeks (Brunauer-Emmett-Teller

202   theory) was determined using a surface area and pore size analyzer (mod. Coulter SA 3100,

203   Beckman Coulter, Fullerton, USA). Weighed quantities of the resulting precipitates were

204   dissolved in 30% HNO_3, and the Eu^{3+} concentration for each sample was determined using ICP-

205   MS (NexION 350 X, PerkinElmer).

206   *Solution Chemistry Analysis*. The pH was measured using a Mettler Toledo Inlab® electrode and

207   calibrated with pH = 4, 6, and 9 standard solutions (WTW, Weilheim, Germany). Ammonium-

208   ammonia concentration was determined using an ammonium ion selective electrode with

209   Nernstian response and measured against a calibration curve (WTW, Weilheim, Germany).

210   Supernatants collected were acidified with HNO_3 (1 %), and Eu^{3+} and Ca^{2+} concentrations were

211   determined using an ICP-MS. All measurements were made in triplicates.

212   **RESULTS**

213   **Biomineralization Precipitation Experiments.** In mineralizing medium containing Eu^{3+} and

214   urea, *S. pasteurii* demonstrated ureolytic behavior consistent with the liteature.[6,13,20] As shown in

215   Figure 1A, pH and NH_4^+ concentrations increased rapidly within the first 6 hours and reached

216   maximum values after 48 hours of 9.2 and 1.0 mol/L, respectively. The decrease of NH_4^+

217   concentrations over time was caused by the release of $NH_3(g)$ in equilibrium with NH_4^+ at this

218   pH. An initial increase in pH of the abiotic control was observed reaching pH = 7.2 after 24

219   hours, although no significant amount of paralleled NH_4^+ production was detected. Notably,

220   induced mineral precipitation was consistently observed in the bacterial samples under these

221   conditions after 3 to 4 hours of reaction time between the pH range of 7.8 and 8.0. For the abiotic

222   control samples, no mineral precipitation was observed throughout the duration of the

223   experiment. This trend was also evident when tracking soluble Ca^{2+} and Eu^{3+} concentrations.

224
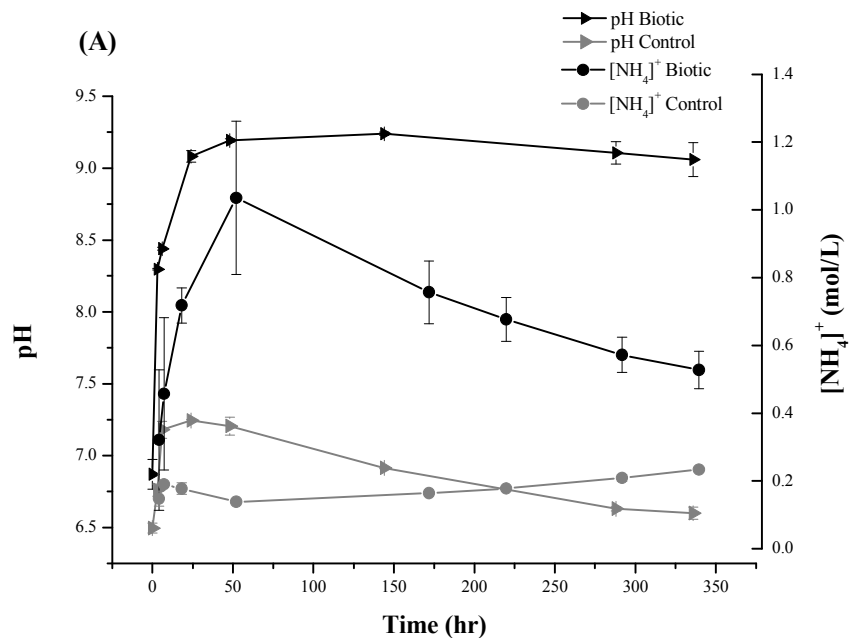
225
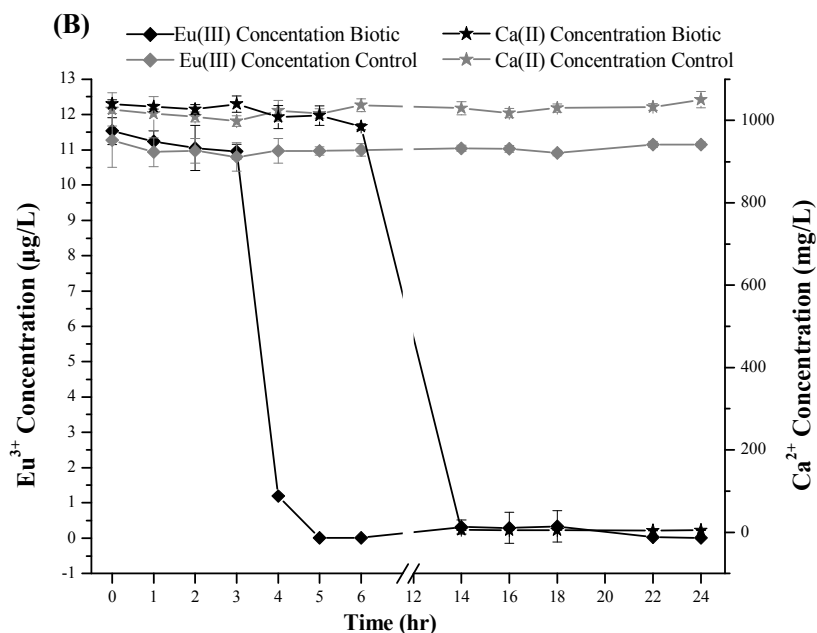
226

227 **Figure 1.** (A) Measured pH and total NH_4^+ in solution in biotic (black triangles and black circles,

228 respectively) and control (grey triangles and grey circles, respectively) cultures as a function of

229 time. (B) Eu^{3+} and Ca^{2+} concentrations measured in the solution in biotic (black diamonds and

230 black stars, respectively) and control (grey diamonds and grey stars, respectively) cultures as a

231 function of time. Points represent the average of triplicate measurements and error bars represent

232 the standard deviation.

233 The change in soluble Eu^{3+} and Ca^{2+} concentrations was tracked and measured by ICP-MS as

234 shown in Figure 1B. In the cultures containing *S. pasteurii*, no drastic consumption of either Ca^{2+}

235 or Eu^{3+} was observed in the first 3 hours of the experiment. After this "induction phase,"

236 europium concentration in solution decreased rapidly. To note, the earlier onset of the decrease

237 in Eu^{3+} does indicate precipitation of a Eu^{3+} solid phase. A significant decrease in Ca^{2+}

238 concentration did not occur until later between the 6th and 14th hours of the experiment.

239 Concentrations of Eu^{3+} and Ca^{2+} reached 0.01 µg/L and 4.35 mg/L and were stabilized after 5

240 and 14 hours, respectively, and no leaching of Eu^{3+} was observed following precipitation.

241 Conversely, in the abiotic control the concentrations of both elements remained constant and the

242 formation of any precipitates was not observed.

243 **Mineral Characterization.** *Particle Formation and Morphology*. Light microscopy was used to

244 monitor the precipitation of biogenic $CaCO_3$ examining morphology, size, and distribution of the

245 mineral. Figure S1 (Supplementary information) displays images of the formation and

246 crystallization of biomineralized $CaCO_3$ at various times over a two-week period. Initial samples

247 collected after three hours show small, undefined precipitates surrounding and closely associated

248 with the bacteria. After six hours, precipitates were observed with discrete shapes ranging in size

249 from 10 to 40 µm. After one day, precipitates ranging up to 50 µm were present exhibiting

250 framboidal morphology. After one and two weeks, precipitates were found ≤ 50 µm in diameter

251 with defined faces and edges. The average surface area per mass of the bulk precipitate collected

252 after two weeks was measured by BET to be 0.42 ± 0.02 m^2/g.

253   SEM was employed to better understand the formation and development of the precipitate

254   morphology from particle to aggregate level. In Figure 2A, the image of precipitate harvested

255   after one day shows small particles with distinct spherical shapes consistent with the vaterite

256   morphology. Other morphologies, e.g., anhedral irregular, hemi-spherulite, and discoid, that have

257   been reported[43] for biogenic carbonates were also found here. On the surfaces of some of the

258   precipitates, pitting resembling bacteria morphology was observed. After one and two weeks

259   (Figure 2B-D), precipitate morphologies were more euhedral/subhedral and resembled those

260   reported for calcite with characteristic rhombohedral faces. In addition, particle size distribution

261   of these precipitates ranged from approximately 2 to 150 μm. EDX analyses of the precipitates

262   (Figure S2) yielded C, O, and Ca as expected for $CaCO_3$. Comparatively small amounts of P and

263   Mg were also identified that most likely originate from the cellular composition of the bacteria.

264   The sensitivity of the EDX analyses was not high enough to detect Eu^{3+} at the concentration

265   used. A weighed quantity of each of the precipitates was dissolved and the Eu^{3+} concentration

266   was measured by ICP-MS. The concentrations after one day, one week, and two weeks were

267 470 ± 47 μg g^{-1}, 546 ± 55 μg g^{-1}, and 531 ± 53 μg g^{-1} Eu^{3+}, respectively.

268

269
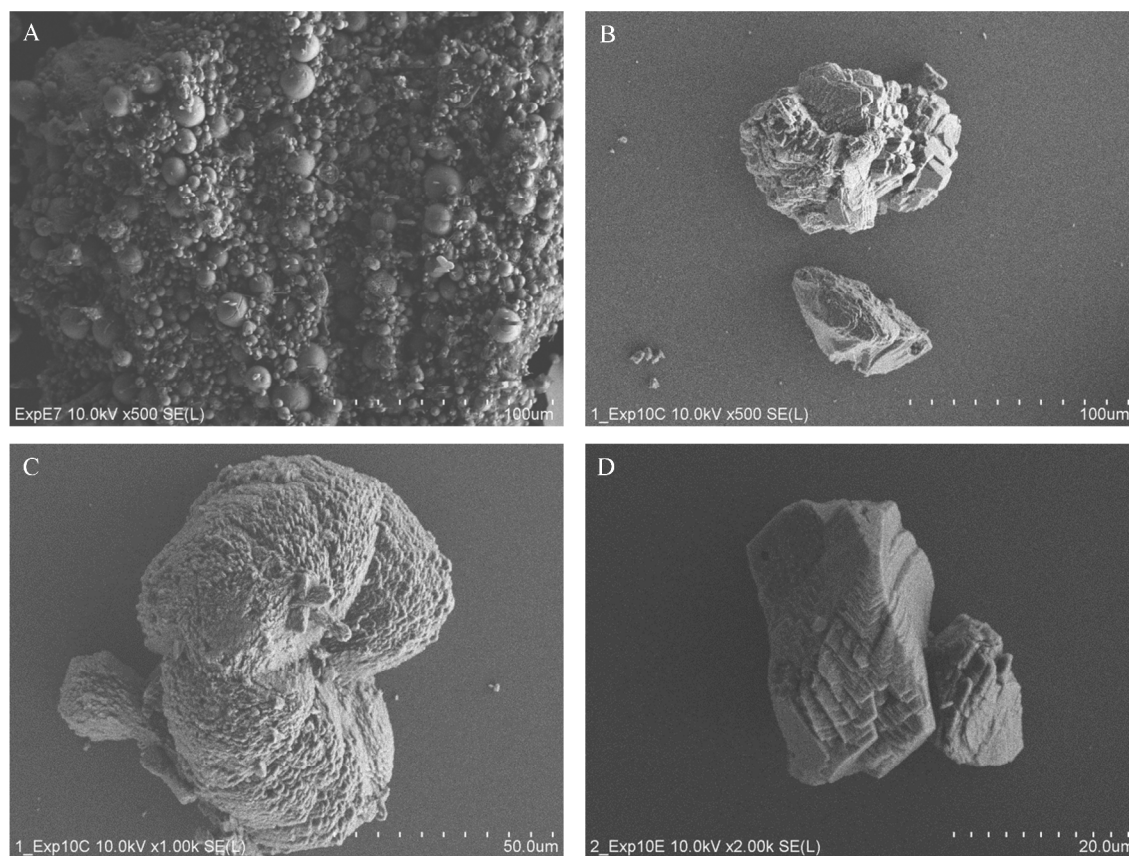
Figure 2. SEM images of biogenic $CaCO_3$ at various times: A) 24 hours, B and C) 1 week, and D) 2 weeks. Scale bars provided at the lower right hand of each image.

Particle Composition Analysis. The mineralogical compositions as a function of time were characterized by powder XRD. As shown in Figure 3, the relative abundance of the identified phases, i.e., vaterite and calcite, of the biogenic $CaCO_3$ changed over time. Vaterite was the predominant phase found after 24 hours, and although the (104) peak of calcite was also observed, it was very weak indicating calcite was a minor phase at this time. After one week the sample also exhibited a mixture of vaterite and calcite, but with calcite as the major constituent. Using the XRD method reported by Dickinson and McGrath[44] for estimating relative phase compositions, the samples were found with 9 ± 5 wt% calcite and 91 ± 5 wt % vaterite after one day and 85 ± 5 wt% calcite and 15 ± 5 wt% vaterite after one week. The complete transformation

281   to calcite was observed after 2 weeks. The phases present at the respective times were consistent

282   with morphologies observed by imaging techniques (Figure 2). For the abiotic precipitate after

283   10 days, a relative phase composition of 14 ± 5 wt% calcite and 86 ± 5 wt% vaterite was

284   determined.
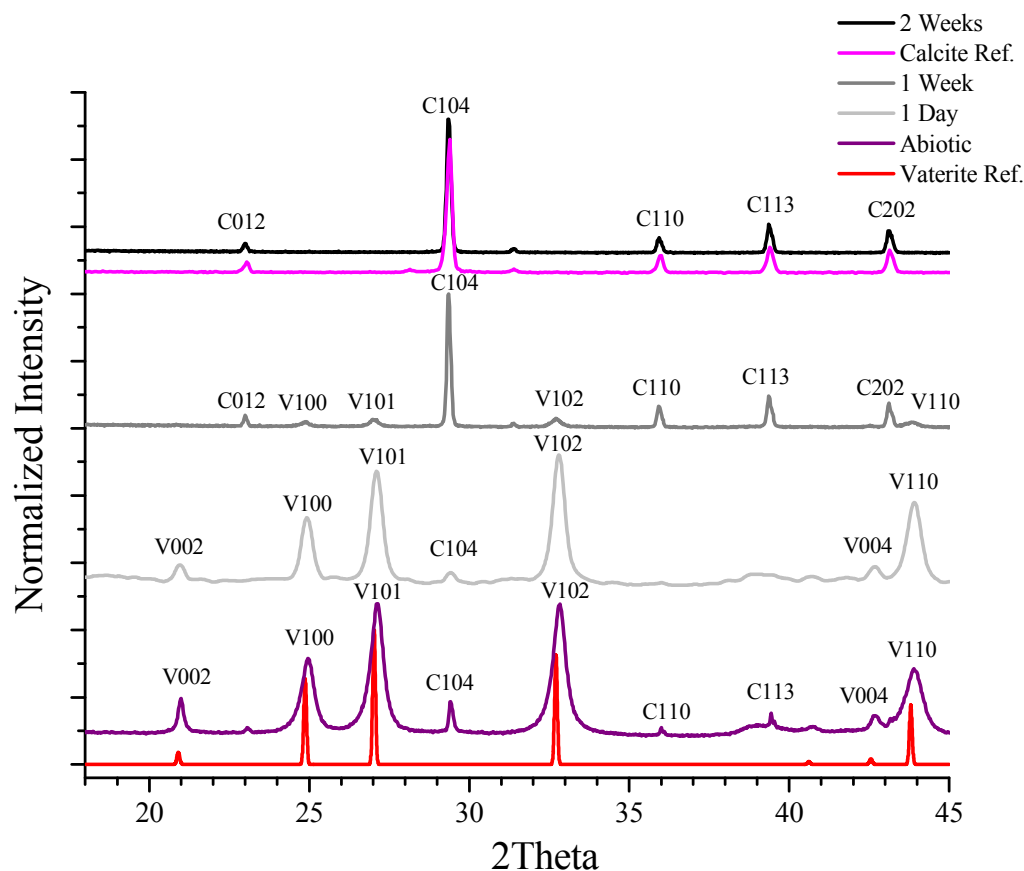
285

286   **Figure 3.** A comparison of XRD powder patterns of biomineralized $CaCO_3$ from *S. pasteurii*

287   after one day, one week, and two weeks, and abiotic $CaCO_3$ after 10 days. Peaks are labeled with

288   the calcite (C) or vaterite (V) and the respective Miller indices [HKL].

289   Thermal gravimetric analysis was used to determine the amount of remaining organic material in

290   the precipitate after recovery and washing. Figure S4 displays the thermal behavior of samples

291   precipitated at different times versus a calcite standard. In comparison with an abiotic calcite

292   standard, which showed no significant loss of mass before ~ 750 ºC, a two-step change in mass

293   in this range was observed for the biogenic $CaCO_3$ samples. This can be attributed to the loss of

294   water associated with the mineral up to 200 ºC, and the loss of organic material from 200 to

295   650 ºC.[45] From this, it was determined that the sample after one day contained about 6 wt%

296   organic matter, whereas the one and two week samples contained about 2 wt%. Final

297   decomposition temperatures of $CaCO_3$ to CaO and CO_2 were approximately 795, 818, and

298   837 ºC for the $CaCO_3$ after one day, two weeks, and one week, respectively. These

299   decomposition temperatures were notably lower than the calcite standard measured at 842 ºC.

300   This has been attributed to the presence of crystal defects due to crystal grain growth speed and

301   the inclusion of trace elements, e.g., Mg^{2+}, into the lattice during crystallization, which can

302   distort and lower the stability of the crystal lattice.[46,47]

303   **Europium TRLFS: Analysis and Speciation.** *Precipitate After One Day.* The excitation

304   spectrum of the Eu^{3+} doped biogenic $CaCO_3$ after one day is shown in Figure 4. In the spectrum,

305   only a single absorption maximum was observed at 579.1 nm corresponding to one species,

306   which will be designated as Species I. The luminescence lifetime of Species I (Table 1, Figure

307   S4) was measured after selective excitation at 579.1 nm and characterized by monoexponential

308   behavior with a value of $\tau = 4550 \pm 580$ µsec. This lifetime value is consistent with 0

309   coordinating H_2O molecules and incorporation of Eu^{3+} in the mineral phase. For the emission

310   spectrum (Figure 5), a two-fold splitting of the $^5D_0 \rightarrow {}^7F_1$ and a three-fold splitting of the

311      $^5D_0 \rightarrow {}^7F_2$ transitions were observed. Comparatively, the emission spectrum and lifetime are

312   consistent with the Eu^{3+} incorporated vaterite species substituted at the Ca^{2+} site.[32]

313
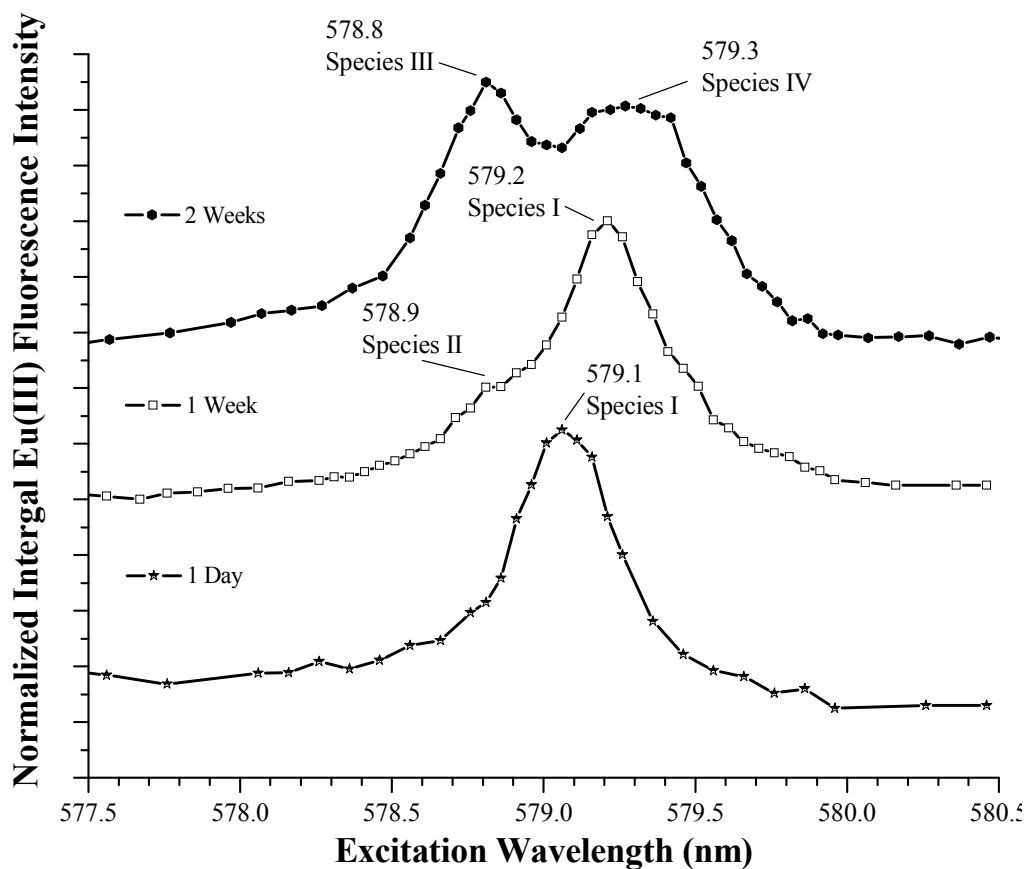
Figure 4. The $^{7}F_{0} \rightarrow {}^{5}D_{0}$ excitation spectra of the Eu^{3+} containing biogenic $CaCO_3$ produced by

315 *S. pasteurii.*

316 *Precipitate After One Week.* After one week, two different excitation species were observed

317 (Figure 4). The speciation here is still dominated by Species I, which exhibited an identical

318 emission spectrum and lifetime compared to the same species after one day. Its excitation

319 maximum had shifted, however, to 579.2 nm. This is explained by spectral overlap with a second

320 species as a much less intense shoulder at 578.9 nm.

321 The shoulder located at 578.9 nm is unique and must be indicative of the presence of a second

322 species, which will be referred to as Species II. Excitation at 578.9 nm yielded a characteristic

323   biexponential fluorescence decay behavior, a property when multiple species are simultaneously

324   excited. A biexponential fit was used and a short and a long component could be derived as

325    $\tau_1 = 1100 \pm 140$ μsec and $\tau_2 = 4070 \pm 530$ μsec, respectively. The long component is identical

326   within the errors of measurement for the lifetime of Species I, hence the short lifetime must be

327   characteristic for Species II. Using Horrock's equation, the value of the short lifetime is

328   equivalent to ~0.5 H_2O molecules coordinated to the Eu^{3+}. This slight hydration suggests that

329   Species II occurs within the solution-solid interface, although primarily still bound within the

330   mineral. Species II can be compared with the transition species identified by Schmidt et. al

331   shown in Table 1.[32] The emission spectrum (Figure 5) of Species II is characterized by both a $^7F_1$

332   and a $^7F_2$ band with a four-fold splitting. In particular, the magnitude of splitting of the $^7F_1$ band

333   exceeds the maximum number of possible $(2J + 1)$ sublevels, which again indicates that multiple

334   species have been simultaneously excited at this wavelength. These results are also consistent

335   with the multiexponential lifetime decay pattern.

336

337 **Table 1.** Fluorescence emission lifetimes of Eu^{3+} species found in biogenic and abiotic

338 precipitates synthesized in mineralization medium (italics, this study) vs. abiotic vaterite[32] and

339 calcite[49].

Species	$\lambda_{excit.}$ (nm)	Lifetime (µsec)	$n(H_2O)$
Species I, One day	*579.1*	*4550 ± 580*	*0*
Species I, One week	*579.2*	*4330 ± 560*	*0*
Species II	*578.9*	*1100 ± 140*	*0.5*
Species III	*578.8*	*2780 ± 360*	*0*
Species IV	*579.3*	*3380 ± 300*	*0*
Abiotic Precipitate	*579.5*	*2040 ± 260*	*0*
*Vaterite Incorporated	579.3	4069 ± 244	0 [32]
*Transition Species	579.1	1106 ± 133	0.5 [32]
**Calcite Sorption A	578.1	412 ± 49	1-2 [49]
**Calcite Incorporated B	578.4	4368 ± 524	0 [49]
**Calcite Incorporated C	579.6	4352 ± 261	0 [49]

340 * Vaterite samples were precipitated by bubbling $CO_2(g)$ through a $CaCl_2$ (1 M) and NH_4OH (2
341 M) solution containing 20 ppm Eu^{3+} and suspended in a $CaCO_3$ saturated solution for vaterite to
342 calcite transformation.
343 ** Calcite samples were produced in a mixed-flow reactor with a calcite seed crystal and input
344 solutions of $Ca(ClO_4)_2$ (2 mM), $NaHCO_3$ (1.8 mM)/Na_2CO_3 (0.15 mM), and Eu^{+3} (~ 10^{-7} M).
345

346 *Precipitate After Two Weeks*. Two defined excitation peaks were identified in the sample after

347 two weeks shown in Figure 4: a peak at 578.8 nm and a broad peak centered at 579.3 nm. The

348 species at 578.8 nm exhibited a long lifetime of 2780 ± 360 µs with a monoexponential decay

349 profile. This value corresponds to a complete loss of hydration. The correlating emission

350 spectrum shown in Figure 5 is characterized by a six-fold split $^7F_1$ band and a $^7F_2$ band with a

351 minimum of five-fold splitting. Again, this magnitude of splitting is consistent with the

352 excitation of multiple species. Notably, this species at 578.8 nm is unique from the other species

353 identified here and those in prior TRLFS studies of the Eu^{3+}-$CaCO_3$ system, hence it will be

354   referred to as Species III. It is speculated that Species III represents Eu^{3+} incorporated within a

355   low symmetry site in the calcite, although its precise local environment cannot be specified.

356   The lifetime of the species at 579.3 nm was measured with a value of 3380 ± 300 μsec, which is

357   consistent with a complete loss of hydration and Eu^{3+} incorporation. A two-fold splitting and

358   three-fold splitting of the $^{7}F_1$ and $^{7}F_2$ band, respectively, are observed in the emission spectrum

359   (Figure 5). This splitting pattern is characteristic of Eu^{3+} incorporated into the trigonal C_{3i} Ca^{2+}

360   site within the calcite lattice.[32-34,49] The lifetime value and emission spectrum of this species is

361   significantly different to the other species in this study, and therefore will be referred to as

362   Species IV. However, it is noted that Species IV is the same species as Species C identified in

363   previous TRLFS investigations of Eu^{3+} with calcite (Table 1 and Figure 5), which has been

364   described as Eu^{3+} substituting Ca^{2+} on a nearly undistorted lattice site.[32-34,49] Because of the

365   broadness of the peak, excitations at 579.2 nm and 579.5 nm were also performed to ensure only

366   one species was present. The results from excitation at these wavelengths were identical with

367   those at 579.3 nm.

368   It is noteworthy that no calcite surface sorption species were observed in the precipitates after

369   one and two weeks. The second calcite incorporation species, Species B, which has been

370   reported in the literature, was also not identified (Table 1).[32,33,49]

371   *Abiotic Precipitate After 10 Days.* As recent investigations have shown, the growth medium may

372   have a significant impact on the calcite surface,[48] and the uptake of trivalent cations by the

373   mineral.[39] To confirm the findings made in this study were due to microbial activity and not the

374   growth medium, mineral was precipitated from the growth medium in the absence *S. pasteurii*

375   and analyzed by TRLFS. The excitation spectrum (Figure S5) of the abiotic precipitate after 10

376   days was measured and a single, broad peak centered at approximately 579.5 nm was identified.

377   Excitation at 579.5 nm yielded a luminescent lifetime of 2040 ± 260 μsec (Table 1), which

378   equates to 0 H_2O molecules in the coordinating sphere the Eu^{3+} species and incorporation into

379   the mineral. The emission spectrum shown in Figure S6 is characterized by a three-fold split $^7F_1$

380   band and a $^7F_2$ band with a minimum of four-fold splitting. From the lifetime and emission data,

381   this Eu^{3+} species can be interpreted as being incorporated into the bulk of the mineral, although

382   in a low-symmetry site. Notably, this species is unique in comparison to Species III and the other

383   species identified in this study as well as those identified in previous TRLFS studies. Therefore,

384   it is difficult to speculate if Eu^{3+} incorporation occurs in the vaterite or calcite phase, however,

385   these results demonstrate the bacteria can affect Eu^{3+} speciation differently than just the medium.
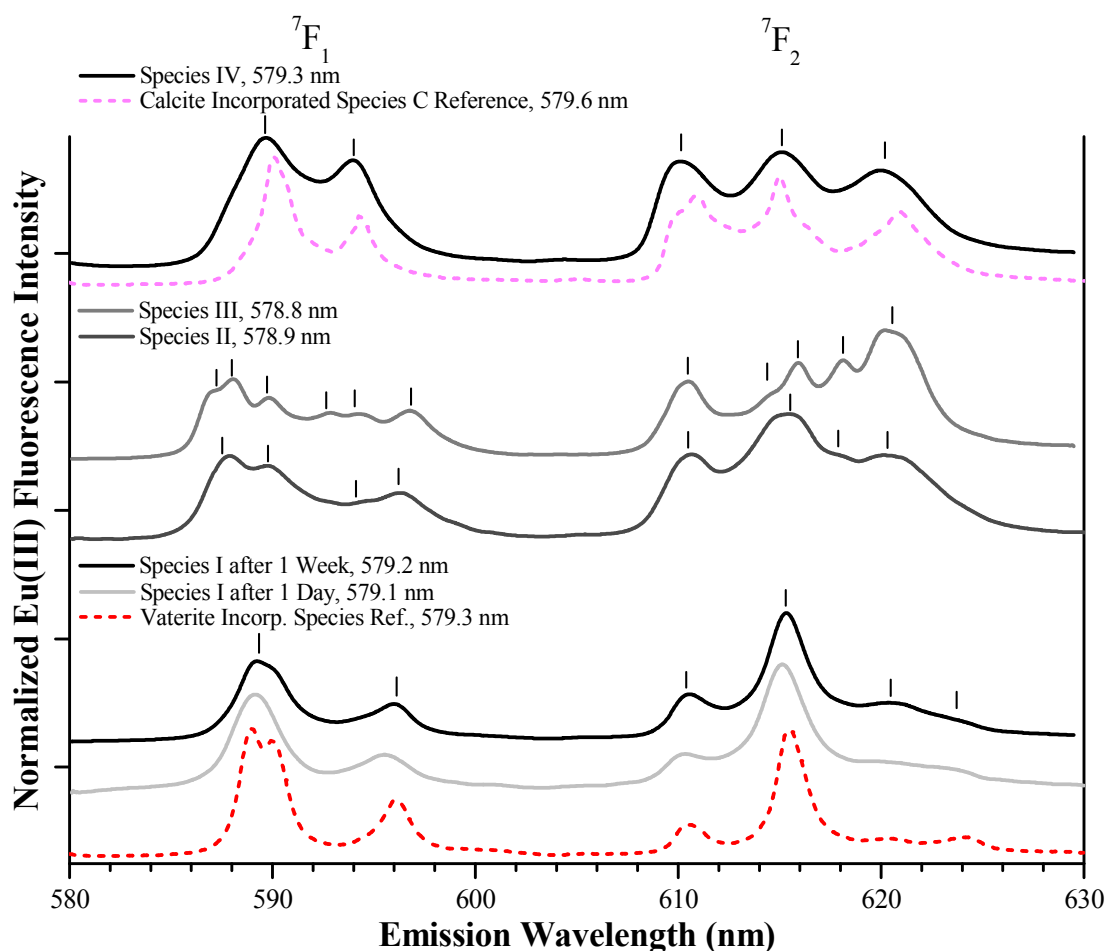
386

387   **Figure 5.** The $^5D_0 \rightarrow \, ^7F_{1,2}$ emission spectra collected from the site-specific excitation of Eu^{3+} in

388   biomineralized $CaCO_3$. Black dash marks indicate splitting peaks.

389

390   **DISCUSSION**

391   In the presence of Eu^{3+}, *S. pasteurii* demonstrated capable ureolytic activity under the

392   experimental conditions consistent with the literature.[6,13,20] This yielded a significant increase in

393   alkalinity of the growth medium, which could be measured by both pH and $[NH_4^+]$. The NH_4^+

394   resulting from ureolysis buffered the medium at pH = 9.2, a pH substantially more alkaline than

395   necessary for $CaCO_3$ precipitation, i.e., pH ~ 8.3.[6] The uptake of free Ca^{2+} and Eu^{3+} ions

396   coincided with $CaCO_3$ precipitation and both were essentially depleted from solution after 14

397   hours. TRLFS results showed no surface sorbed Eu^{3+} species present with either the vaterite or

398   calcite after one day. Surface sorbed species have been reported in batch and mixed-flow studies

399   with inorganic $CaCO_3$ where surface interactions of Eu^{3+} with the mineral occur before

400   incorporation.[32,34,49] This suggests that the Eu^{3+} was either co-precipitated with the $CaCO_3$ or

401   completely incorporated into the vaterite after one day. After the onset of precipitation, the

402   bacterium and small aggregates of the mineral were in close association, providing evidence for

403   bacterial involvement during the mineralization process.[6] The resulting precipitates were

404   characteristic of biogenic vaterite and calcite and contained between 2 to 6 weight percent of

405   organic material as well as trace element inclusions such as Mg and P.

406   At least up to one week, Eu^{3+} was found preferentially incorporated in the vaterite phase (i.e.,

407   Species I), or to a lesser degree as a transition species (i.e., Species II), at the mineral-solution

408   interface. Notably, no Eu^{3+} was found associated with the calcite phase, even with it being the

409   predominate phase present in the mineral composition after one week. These trends suggest that

410   the incorporation of Eu^{3+} in biogenic vaterite undergoes slower phase transformation to calcite in

411   comparison to vaterite without Eu^{3+}. The presence of a hydrated transition species confirms that

412   the phase transformation from vaterite to calcite is a solution-mediated process and is consistent

413   with the literature.[32]

414   In this study, no sorption species were identified within the timeframe of the experiment. The

415   formation of surface sorbed species with calcite has been identified in mix-flowed reactor and

416   batch studies resulting from mineral dissolution-reprecipitation under steady-state and mineral

417   growth conditions.[32,34,49] This is likely attributed to the lower mineral solubility,[8] which would

418   also prevent significant leaching of either Ca^{2+} or Eu^{3+} after mineral precipitation, observed

419   under these conditions. Previous studies have shown that MICP minerals can behave notably

420   different than their abiotic counterparts due to organic and trace element inclusions and high

421   variability in mineral morphologies and surface topologies originating from their biogenic

422   formation.[50,51]

423   A new Eu^{3+} species, Species III, was identified in the calcite phase incorporated in a low-

424   symmetry environment. This species was not identified in the abiotic sample, nor has it been

425   reported in previous Eu^{3+} TRLFS studies with calcite. The literature has shown that the origin of

426   the mineral can significantly impact the possible interactions of doping elements within the

427   mineral, such as for the bioapatite system.[36,37] Considering the mineral composition, it is

428   speculated that Species III could reside in the organic matrix, organic-mineral interface, and/or

429   another low-symmetry coordination environment in the calcite. However, the presence of

430   Species IV, which is incorporated at the Ca^{2+} site in the lattice, also demonstrates that the

431   substitution of Eu^{3+} for Ca^{2+} is still thermodynamically favored under these conditions.[32-34,49]

432   Ultimately, both Species III and Species IV are incorporated and essentially sequestered within

433   the calcite precipitate. When considering contaminate retardation or removal in natural or

434   engineered environmental systems, this geochemical behavior is quite favorable.

435   In the abiotic precipitate, a mixture of vaterite and calcite was obtained, and a single low-

436   symmetry, incorporated species was identified by TRLFS. However, because this species has not

437   been identified in previous studies or in the biogenic samples produced here, it cannot be

438   definitively stated in which phase this species is incorporated. It is well-known that growth

439   medium and synthetic conditions can have a significant impact on mineral phase, morphology,

440   stability, etc.[52] during $CaCO_3$ precipitation, whereas the effect they might have on speciation of

441   co-contaminants present during mineral formation has been considerably less studied. Although,

442   recent investigations have shown that nitrate present even in trace amounts ($\sim 10^{-7}$ M) in the

443   medium can effectively alter Eu^{3+} interactions and speciation with $CaCO_3$.[39] Future research

444   should be aimed at also better understanding these phenomena.

445   The results presented here demonstrate that biomineralized $CaCO_3$ arising from MICP is capable

446   of sequestrating Eu^{3+}, and hence this system should also behave similarly for other trivalent

447   lanthanides and trivalent actinides. These findings reiterate that the interactions of these elements

448   with minerals can be affected by the provenance and the conditions under which the mineral is

449   formed. Thus, the unique interaction of biomineralized $CaCO_3$ with Eu^{3+} solidifies the need to

450   further explore the role of biologically formed minerals in the near and far field of nuclear

451   repository sites and how they interact with (radio)contaminants. It also demonstrates the

452   importance of molecular level studies of diverse systems to be able to reliably describe (and

453   predict) the behavior of biogeochemical systems.

454 ASSOCIATED CONTENT

455 **Supporting Information**. Light microscope images of precipitates and graphs of TGA, EDX,

456 TRLFS lifetime measurements of biogenic $CaCO_3$ with Eu^{3+} samples, and TRLFS excitation

457 spectrum of calcite produced without bacteria are provided. This material is available free of

458 charge via the Internet at http://pubs.acs.org.

459 AUTHOR INFORMATION

460 **Corresponding Author**

461 E-mail: moritz.schmidt@hzdr.de (MS), Phone: +49-351-260 3136

462 **Notes**

463 The authors declare no competing financial interest.

471 REFERENCES

472 1. Lowenstam, H. A.; Weiner, S. In *On Biomineralization*. NewYork, NY: Oxford University

473   Press, **1989**.

474   2. Decho, A. W. Overview of biopolymer-induced mineralization: what goes on in biofilms?

475   *Ecol. Eng*. **2010**, *36*: 137-144.

476   3. Benzerara, K.; Miot, J.; Morin, G.; Ona-Nguema, G.; Skouri-Panet, F.; Ferard, C.

477   Significance, mechanisms and environmental implications of microbial biomineralization.

478   *CR: Geosci*. **2011**, *343*, 160-7.

479   4. Dhami, N. K.; Reddy, M. S.; Mukherjee, A. Biomineralization of calcium carbonates and

480   their engineered applications: a review. *Frontiers in microbiology* **2013**, *4*, 314.

481   5. Sarayu, K.; Iyer, N. R.; Murthy, A. R. Exploration on the biotechnological aspect of the

482   ureolytic bacteria for the production of the cementitious materials--a review. *Appl. Biochem.*

483   *Biotech.* **2014,** *172* (5), 2308-23.

484   6. Stocks-Fischer, S.; Galinat, J. K.; Bang, S. S. Microbiological precipitation of $CaCO_3$. *Soil*

485   *Biol. Biochem*. **1999**, *31*, 1563–1571.

486   7. Fujita, Y.; Ferris, F. G.; Lawson, R. D.; Colwell, F. S.; Smith, R. W. Calcium carbonate

487   precipitation by ureolytic subsurface bacteria. *Geomicrobiol. J.* **2000,** *17* (4), 305-318.

488   8. Mitchell, A. C.; Ferris, F. G. The influence of Bacillus pasteurii on the nucleation and growth

489   of calcium carbonate. *Geomicrobiol. J.* **2006,** *23* (3-4), 213-226.

490   9. Lauchnor, E. G.; Schultz, L. N.; Bugni, S.; Mitchell, A. C.; Cunningham, A. B.; Gerlach, R.

491   Bacterially induced calcium carbonate precipitation and strontium coprecipitation in a porous

492   media flow system. *Environ. Sci. Technol.* **2013,** *47* (3), 1557-64.

493   10. Achal, V.; Pan, X. Influence of calcium sources on microbially induced calcium carbonate

494   precipitation by Bacillus sp. CR2. *Appl. Biochem. Biotech.* **2014,** *173* (1), 307-17.

495   11. Burne, R. A.; Chen, Y. M. Bacterial ureases in infectious diseases. *Microbes and Infection*.

496   **2000**, *2,* 533-42.

497   12. Parks, S. L. Kinetics of Calcite Precipitation by Ureolytic Bacteria under Aerobic and

498   Anaerobic Conditions. MS Thesis. **2009**, Montana State University, Bozeman MT.

499   13. Warren, L. A.; Maurice, P. A.; Parmar, N.; Ferris, F. G. Microbially mediated calcium

500   carbonate precipitation: implications for interpreting calcite precipitation and for solid-phase

501   capture of inorganic contaminants. *Geomicrobiol. J.* **2001,** *18* (1), 93-115.

502   14. Rodriguez-Navarro, C.; Jimenez-Lopez, C.; Rodriguez-Navarro, A.; Gonzalez-Muñoz, M.

503   T.; Rodriguez-Gallego, M. Bacterially mediated mineralization of vaterite. *Geochim.*

504   *Cosmochim. Ac*. **2007,** *71* (5), 1197-1213.

505   15. Phillips, A. J.; Gerlach, R.; Lauchnor, E.; Mitchell, A. C.; Cunningham, A. B.; Spangler, L.

506   Engineered applications of ureolytic biomineralization: a review. *Biofouling*. **2013**, *29* (6),

507   715-33.

508   16. Martin, D.; Dodds, K.; Butler, I. B.; Ngwenya, B. T. Carbonate precipitation under pressure

509   for bioengineering in the anaerobic subsurface via denitrification. *Environ. Sci. Technol*.

510   **2013,** *47* (15), 8692-9.

511   17. Kang, C. H.; Han, S. H.; Shin, Y.; Oh, S. J.; So, J. S. Bioremediation of Cd by microbially

512   induced calcite precipitation. *Appl. Biochem. Biotech.* **2014,** *172* (6), 2907-15.

513   18. Kang, C. H., Oh, S. J., Shin, Y., Han, S., Nam, I. (2015). "Bioremediation of lead by

514   ureolytic bacteria isolated from soil at abandoned metal mines in South Korea."Ecol. Eng.

515   **2015**, *74*, 402-407.

516   19. Fujita, Y.; Redden, G. D.; Ingram, J. C.; Cortez, M. M.; Ferris, F. G.; Smith, R. W. Strontium

517   incorporation into calcite generated by bacterial ureolysis. *Geochim. Cosmochim. Ac*. **2004,**

518   *68* (15), 3261-70.

519   20. Fujita, Y.; Taylor, J.; Wendt, L.; Reed, D.; Smith, R. Evaluating the potential of native

520   ureolytic microbes to remediate Sr contaminated environment. *Environ. Sci. Technol*. **2010**,

521   *44*, 7652–8.

522   21. Mitchell, A. C.; Ferris, F. G. The coprecipitation of Sr into calcite precipitates induced by

523   bacterial ureolysis in artificial groundwater: Temperature and kinetic dependence. *Geochim.*

524   *Cosmochim. Ac*. **2005,** *69* (17), 4199-4210.

525   22. Aarkog, A.; Lippert, J. Europium-155 in debris from nuclear weapons. *Science*. **1967**,

526   *157(3787)*, 425-427.

527   23. Geckeis, H.; Lutzenkirchen, J.; Polly, R.; Rabung, T.; Schmidt, M. Mineral-water interface

528   reactions of actinides. *Chem. Rev.* **2013,** *113* (2), 1016-62.

529   24. Thein, M.; Beck, J. N.; Johnson, H.; Cooper, W. W.; Reynolds, M. A.; Clark, R. S.; Baugh, J.

530   O.; Kuroda, P. K. Fractionation of [atomic] bomb-produced rare-earth nuclides in the

531   atmosphere. *Environ. Sci. Technol*. **1969**, *3*, 667−670.

532 25. Thakur, P.; Lemons, B. G.; Ballard, S.; Hardy, R. Environmental and health impacts of

533   February 14, 2014 radiation release from the nation's only deep geologic nuclear waste

534   disposal. *J. Environ. Radioact.* **2015**, *146*, 6-15.

535 26. Bunzli, J. C. G.; Piguet, C. Taking advantage of luminescent lanthanide ions. *Chem. Soc.*

536   *Rev.* **2005**, *34*, 1048-1077.

537 27. Martin, R. B.; Richardson, F. S. Lanthanides as probes for calcium in biological systems. *Q.*

538   *Rev. Biophys.* **1979**, I2, 181-209.

539 28. Stumpf, T.; Marques Fernandes, M.; Walther, C.; Dardenne, K.; Fanghanel, T. Structural

540   characterization of Am incorporated into calcite: a TRLFS and EXAFS study. *J Colloid*

541   *Interf. Sci* **2006,** *302* (1), 240-5.

542 29. Stumpf, T.; Fanghanel, T. A time-resolved laser fluorescence spectroscopy (TRLFS) study of

543   the interaction of trivalent actinides (Cm(III)) with calcite. *J Colloid Interf. Sci* **2002,** *249* (1),

544   119-22.

545 30. Lakhstanov, L. Z.; Stipp, S. L. S. Experimental study of europium (III) coprecipitation with

546   calcite. *Geochim. Cosmochim. Ac.* **2004**, *68*, 819-827.

547 31. Elzinga, E. J.; Reeder, R. J.; Withers, S. H.; Peale, R. E.; Mason, R. A.; Beck, K. M.; Hess,

548   W. P. (2002) EXAFS study of rare-earth element coordination in calcite. *Geochim.*

549   *Cosmochim. Ac.* **2002**, *66*, 2875–2885.

550   32. Schmidt, M.; Stumpf, T.; Walther, C.; Geckeis, H.; Fanghanel, T. Phase transformation in

551         $CaCO_3$ polymorphs: a spectroscopic, microscopic, and diffraction study. *J Colloid Interf. Sci*

552   **2010,** *351* (1), 50-56.

553   33. Schmidt, M.; Stumpf, T.; Marques Fernandes, M.; Walther, C.; Fanghanel, T. Charge

554   compensation in solid solutions. *Angew. Chem.* **2008,** *47* (31), 5846-50.

555   34. Piriou, B.; Fedoroff, M.; Jeanjean, J.; Bercis, L. Characterization of the sorption of

556   europium(III) on calcite by site-selective and time-resolved luminescence spectroscopy. *J.*

557   *Colloid Interf. Sci*. **1997**, *194* (2), 440–447.

558   35. Stipp, S. L. S.; Christensen, J. T.; Lakhstanov, L. Z.; Baker, J. A.; Waight, T. E. Rare Earth

559   element (REE) incorporation in natural calcite: Upper limits for actinide uptake in a

560   secondary phase. *Radiochim. Acta.* **2006**, *94*, 523-528.

561   36. Holliday, K.; Handley-Sidhu, S.; Dardenne, K.; Renshaw, J.; Macaskie, L.; Walther, C.;

562   Stumpf, T. A new incorporation mechanism for trivalent actinides into bioapatite: a TRLFS

563   and EXAFS study. *Langmuir.* **2012,** *28* (8), 3845-51.

564   37. Holliday, K. S.; Dardenne, K.; Walther, C.; Stumpf, T. The incorporation of europium into

565   apatite: anew explanation. *Radiochim. Acta.* **2013,** *101* (4), 267-272.

566   38. Schmidt, M.; Stumpf, T.; Walther, C.; Geckeis, H.; Fanghanel, T. Incorporation versus

567   adsorption: substitution of Ca^{2+} by Eu^{3+} and Cm^{3+} in aragonite and gypsum. *Dalton T.* **2009,**

568   *33*, 6645-50.

569   39. Hofmann, S.; Voïtchovsky, K.; Schmidt, M.; Stumpf, T. Trace concentration – Huge impact:

570   Nitrate in the calcite/Eu(III) system. *Geochim. Cosmochim. Ac.* **2014,** *125*, 528-538.

571   40. Binnemans, K. Interpretation of europium(III) spectra. *Coord. Chem. Rev*. **2015**, *295*. 1-45.

572   41. Horrocks, W. D.; Sudnick, D. R. Lanthanide ion probes of structure in biology – laser-

573   induced luminescence decay constants provide a direct measure of the number of metal

574   coordinated water-molecules. *J. Am. Chem. Soc*. **1979**, *101*, 334–340.

575   42. Choppin, G. R.; Jensen, M. P. In *Chemistry of the Actinides and Transactinides*; Morss, L.

576   R., Edelstein, N. M., Fuger, J., Eds.; Springer: Dordrecht, Germany, **2006**; p 2528.

577   43. Ronholm, J.; Schumann, D.; Sapers, H. M.; Izawa, M.; Applin, D.; Berg, B.; Mann, P.; Vali,

578   H.; Flemming, R. L.; Cloutis, E. A.; Whyte, L. G. A mineralogical characterization of

579   biogenic calcium carbonates precipitated by heterotrophic bacteria isolated from cryophilic

580   polar regions. *Geobiology.* **2014,** *12* (6), 542-56.

581   44. Dickinson, S. R.; McGrath, K. M. Quantitative determination of binary and tertiary calcium

582   carbonate mixtures using powder X-ray diffraction. *The Analyst* **2001,** *126* (7), 1118-1121.

583   45. Huaxiao, Y.;Han, Z.; Zhao, H.; Zhou, S.; Chi, N.; Han, M.; Kou, X.; Zhang, Y.; Xu, L.;

584   Tian, C.; Qin, S. Characterization of calcium deposition induced by Synechocystis sp.

585   PCC6803 in BG11 culture medium. *Chinese Jour. Ocean. Limn*. **2014**, *32* (3): 503-510.

586   46. Stalport, F.; Coll, P.; Cabane, M.; Person, A.; González, R. N.; Raulin, F.; Vaulay, M. J.;

587   Ausset, P.; McKay, C. P.; Szopa, C.; Zarnecki, J. Search for past life on Mars: Physical and

588　　　chemical characterization of minerals of biotic and abiotic origin: part 1 - Calcite. *Geophys.*

589　　　*Res. Lett.* **2005,** *32* (23), L23305.

590　47. Astilleros, J. M., C. M. Pina, L. Fernandez-Diaz, and A. Putnis. Metastable phenomena on

591　　　calcite {1014} surfaces growing from Sr^{2+}-Ca^{2+}-CO_3^{2-} aqueous solutions, *Chem. Geol.*, **2002**,

592　　　*193*, 93–107.

593　48. Hofmann, S., Voïtchovsky, K., Spijker, P., Schmidt, M., Stumpf, T. Visualising the

594　　　molecular alteration of the calcite (104) – water interface by sodium nitrate. *Sci. Rep.* **2016**,

595　　　*6*, 21576.

596　49. Fernandes, M. M.; Schmidt, M.; Stumpf, T.; Walther, C.; Bosbach, D.; Klenze, R.;

597　　　Fanghanel, T. Site-selective time-resolved laser fluorescence spectroscopy of Eu^{3+} in calcite.

598　　　*J Colloid Interf. Sci* **2008,** *321* (2), 323-31.

599　50. Gilbert, P. U. P. A.; Abrecht, M.; Frazer, B. H. The Organic-Mineral Interface in

600　　　Biominerals. *Rev. Mineral. Geochem.* **2005**, *59*, 157-185.

601　51. Mann, S. In *Biomineralization: Principles and Concepts in Bioinorganic Materials*

602　　　*Chemistry*. Oxford Univ. Press, Oxford, **2001**.

603　52. Naka, K.; Chujo, Y. Control of crystal nucleation and growth of calcium carbonate by

604　　　synthetic substrates. *Chem. Mater.* **2001**, *13*, 3245-3259.

605

606   TOC

MICP   **TRLFS**
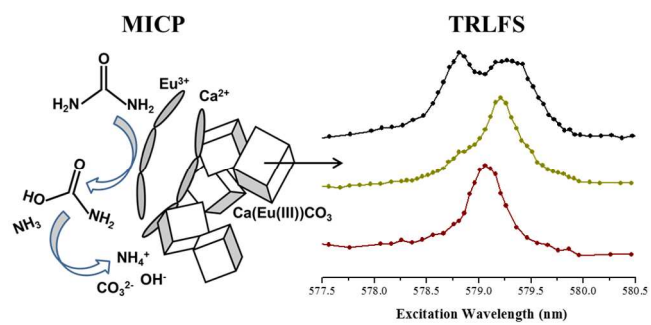
607
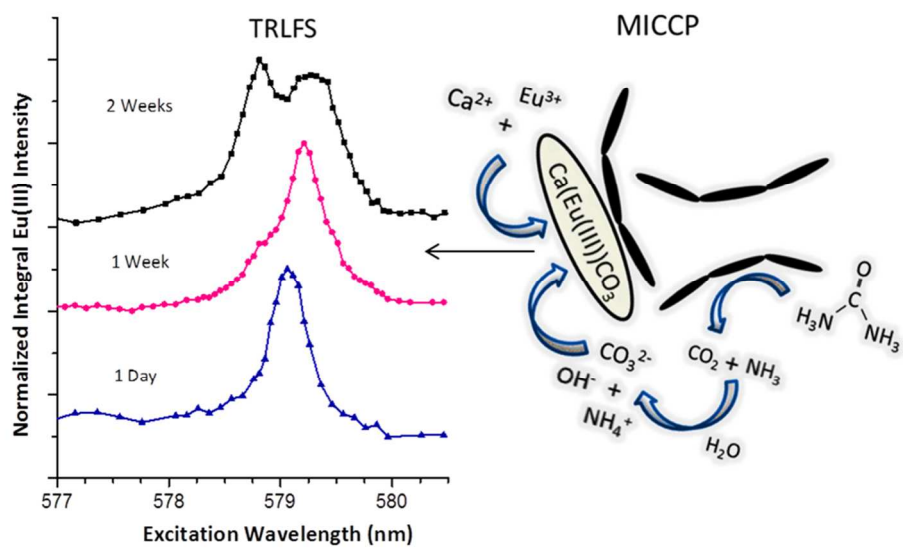
TOC graphic

227x131mm (150 x 150 DPI)